The Impact of Wave Prediction Uncertainty on the Control of a Multi-Axis Wave Energy Converter

Carrie Hall, Yueqi Wu, Igor Rizaev, Wanan Sheng, Robert Dorrell and George Aggidis

Abstract—**As global energy demands and climate concerns continue to grow, the need for renewable energy is becoming increasingly clear and wave energy converter (WEC) systems are receiving growing interest. WECs often utilize optimal control techniques for power take-off operation and leverage a prediction of the upcoming wave force to ensure power production optimization. Prior work has clearly demonstrated that high power production can be achieved when an exact system model is used and the upcoming wave conditions are known, but uncertainty in the underlying model or the wave prediction can degrade performance. The uncertainty in these predictions and the model could degrade the WEC's power output. This work examines the impact of uncertainty on the control of a WEC system that leverages machine learning to predict wave forces over the upcoming time horizon. This paper quantifies wave prediction uncertainty and its seasonal variation and illustrates that this uncertainty may only minimally degrade power output on complex multi-axis WECs due to the strong influence of constraints in the system.**

Index Terms—**wave energy converter, machine learning, wave prediction, model predictive control**

I. Introduction

In order to meet rising energy needs in a sustainable manner, significant growth in renewable electricity production is essential. Solar and wind energy are two commonly considered renewable energy sources, but when solar energy is converted to wave energy at the water surface, the energy intensity increases [1]. This unique feature means that ocean waves could provide an excellent future energy source. While wave energy converters (WECs) have been researched since the 1970s, these systems have not yet reached maturity. In such devices, the maximum energy will be captured if the frequency of the WEC system matches the dominant frequency of the incoming wave. The power take-off (PTO) system can be used to effectively adjust the device frequency. A wide range of PTO systems exist including turbines, hydraulic systems, and linear actuators [2], but in this work a hydraulic PTO is integrated given the cost-effectiveness of this option.

Many strategies for controlling the PTO system have been investigated over the years in an effort maximize energy production. Early strategies often manipulated the PTO system by leveraging linear models and velocity tracking, complex conjugated or impedance matching control. Studies by Hals [3] and later Garcia-Violini [4] compared a variety of these techniques. While these methods have merits, they often encounter challenges with operation over a wide frequency range and can become computational intensive. Those with feedforward components also needed wave excitation estimates and as such, could be more prone to performance problems due to wave prediction errors [4].

WEC control typically aims to maximize energy production, and as such, many strategies have relied on optimal control methods. A wide variety of optimal control strategies have been explored including model predictive control (MPC) [5], [6], spectral and pseudo spectral methods [7], [8], flatness-based [9] and moment-based approaches [10], [11]. Many optimization schemes leverage a model of some type to select the PTO action that optimizes energy production over a future horizon. This approach is logical but has two primary challenges: 1) the need for an accurate WEC model and 2) the need for an estimate of future wave forces.

The need for accurate models is difficult since WECs are complex hydrodynamic systems with nonlinear dynamics but will not be addressed directly in this work. Instead, this paper focuses on uncertainty coming from the predictions of the incoming waves. Methods of wave prediction include models based on stochastic time series based on the previous time steps [12], [13], Gaussian process models [14] or autoregressive models [15]. Fewer studies have considered the uncertainty of the incoming waves in the control methodology. Lao and Scruggs included variability of wave depth assuming it was a stationary stochastic process with a known power spectral density [16]. Stochastic effects on the future wave excitation force were considered

This work was partially supported by the US-UK Fulbright Commission through the Fulbright-Lancaster University Scholar Award 2022-2023. Additional funding was provided by the UK Engineering and Physical Sciences Research Council (EPSRC grant number EP/V040561/1) for the project Novel High-Performance Wave Energy Converters with advanced control, reliability and survivability systems through machine-learning forecasting (NHP-WEC).

Carrie Hall is with the Department of Mechanical, Materials, and Aerospace Engineering at the Illinois Institute of Technology in Chicago, IL, USA 60616 (e-mail: chall9@iit.edu).

Yueqi Wu is with Engineering Department at Lancaster University, Lancaster, UK. (e-mail: y.wu31@lancaster.ac.uk).

Igor Rizaev is with the Energy and Environment Institute at the University of Hull, Hull, UK. (e-mail: i.g.rizaev@hull.ac.uk).

Wanan Sheng is with Engineering Department at Lancaster University, Lancaster, UK. (e-mail: w.sheng@lancaster.ac.uk).

Robert Dorrell is with the University of Hull, Hull, UK. (e-mail: r.dorrell@hull.ac.uk).

George Aggidis is with Engineering Department at Lancaster University, Lancaster, UK. (e-mail: g.aggidis@lancaster.ac.uk).

Digital Object Identifier:
https://doi.org/10.36688/ewtec-2023-453

by Fusco and it was shown that the affect of errors could be attenuated with adjustments to the closed loop transfer function [13]. In other words, if the nature of the uncertainty is known in advance, it can be accommodated. Stochastic control strategies have also been explored to deal with the uncertain nature of the incoming waves [17]–[20].

In recent years, the prevalence of machine learning has enabled another option for predicting incoming wave features. Neural networks can be trained to provide real-time predictions of waves, but they carry with them an uncertainty given the black-box nature of the prediction. Comparisons to physics-based models such as the Simulating WAves Nearshore (SWAN) wave model have shown that machine learning can produce accurate results with less computational burden [21]. Multi-layer ANNs have been successfully used along with an MPC scheme leading to significant improvements in performance particularly in conditions with irregular waves [22], [23].

Based on these prior efforts, this study examines wave predictions for a specific location off the coast of Ireland and Scotland and investigates the impact that these predictions have on control of a constrained WEC system. The TALOS WEC considered in this work has a unique design that should enable higher energy extraction from incoming waves but this design also has some additional constraints to the motion that may in turn limit the controller's ability to optimize energy production. This paper seeks to 1) quantify wave prediction uncertainty and its variation over different locations and seasons, and 2) examine the impact that this real-life uncertainty has on WEC energy output operating with constraints.

II. Wave Data and Measured Wave Variation

In order to examine the impact of wave predictions, wave characteristics were gathered for a location at a longitude of $8.5152°$W and latitude of $55.8919°$N (Figure 1). Characteristics were based on an analysis-forecast numerical wave model (product NORTHWESTSHELF_ANALYSIS_FORECAST_WAV_004_014) from the Copernicus Marine Environment Monitoring Service (CMEMS).

The variation in key wave characteristics at this location were examined including significant wave height, energy wave period, zero-crossing mean wave period, peak period and mean wave direction. Data was available on an hourly basis. This hourly data was used to create higher resolution simulated data sets that represented the same significant wave height and peak period observed over the course of that hour. This allowed the control action to be examined with data that better reflects actual conditions as will be discussed in more detail later. Significant wave height and peak period are focused on here as they directly impact the external wave force on the WEC and as such, will directly impact the control performance to be explored in the next section.

Figures 2 and 3 illustrate the variation observed in significant wave height and peak period observed

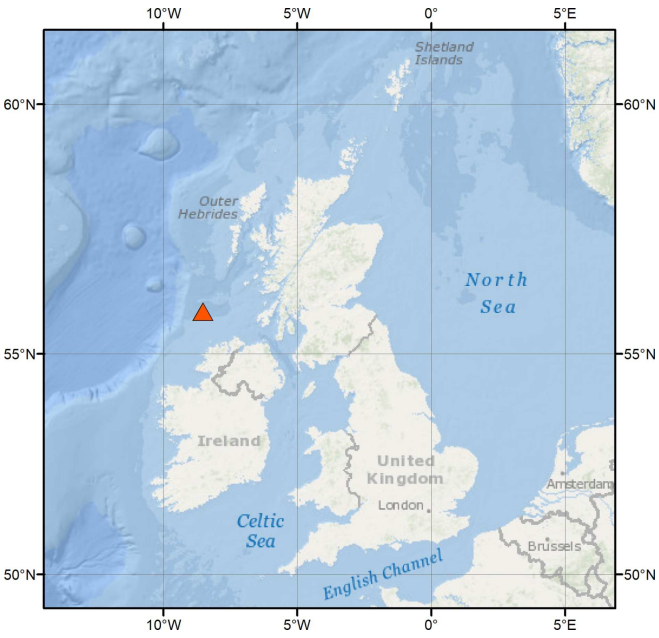

Fig. 1. Test site for wave data off the coasts of Ireland and Scotland

over each month. Average significant wave height is highest from October to March and daily variability is also most significant during these time periods. The summer months have lower wave heights and more steady significant wave heights throughout the course of the day. Peak periods range from 6 to 21 seconds with some days seeing drastic shifts over that range in the course of a day in the winter months. Variations in peak periods are still observed in the summer but the peak periods are shorter with a maximum around 16 seconds.

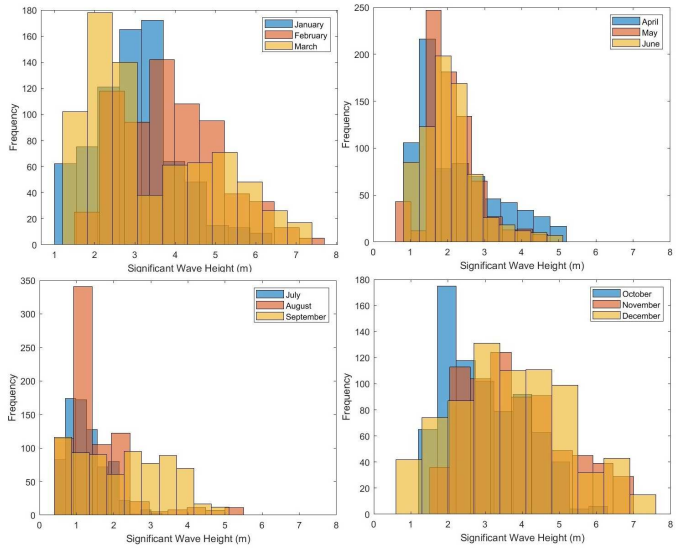

Fig. 2. Variation in significant wave height in 2021

The seasonal and daily variability may be important to consider when using machine learning for wave predictions. Networks that are trained on data from a particular month or time of day only may not capture other times of the year or day well. A preliminary study on this effect will be presented in the next section but further work that leverages more data and higher

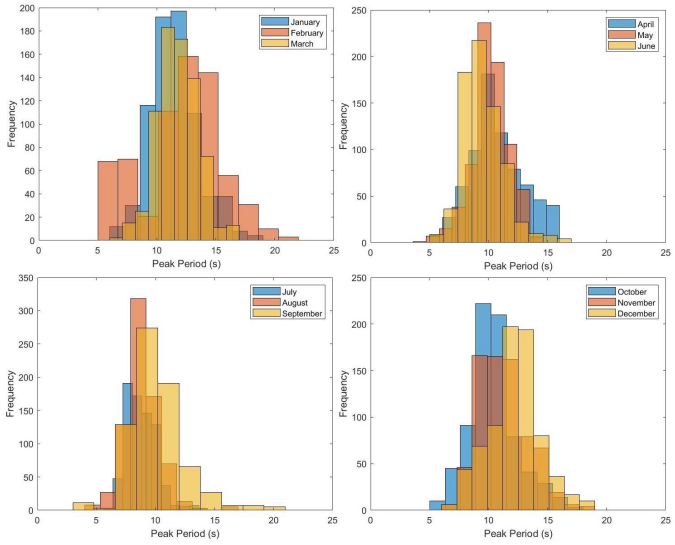

Fig. 3. Variation in peak period in 2021

resolution data would be valuable.

The measured wave statistics were recorded on an hourly basis and data for the 2021 year were used in this study. While hourly characteristics are useful for studies of the wave climate, control methodologies are implemented with a much smaller sampling time. In order to create a representative data set with the resolution needed for control development, these hourly wave characteristics were used to create a wave time series with a 0.05 second resolution that represent an irregular wave with the measured statistical significant wave height and peak period metrics. The wave time series was generated using Inverse Fourier transform from an assumed wave spectrum (Bretschneider) with the wave significant height, and peak period. As such the measurements along with the numerical model provide a prediction of the anticipated wave forces with respect to time at a resolution useful for control development. This data set was used for machine learning based predictions and the evaluation of the impact on control effectiveness.

III. Machine Learning for Wave Predictions

Wave predictions were created using a long short-term memory (LSTM) network that was trained on simulation data for the external wave force and resulting TALOS position, PTO force and power output. The LSTM predictions of the external wave force were based on current observations on-board TALOS. The LSTM had 100 hidden layers and was trained on 80% of the data with the remaining 20% used for validation.

The LSTM was initially trained using 1 hour of 10Hz data for the time from midnight to 1am on January 1, 2021. During this hour, the wave height was 2.968 m and the peak period was 8.60 seconds. As illustrated in Figure 4, the LSTM is able to accurately predict the external wave force based on the on-board TALOS measurements. The errors for the prediction are shown in Figure 5 with most errors being relatively small and maximum errors being around 220kN.

In order to test the capabilities of the network, the network trained on the January 1st data set was used to predict the external wave forces for the 12pm-1pm on July 1, 2021. Wave conditions at that time have a much lower significant wave height of 0.882 m but a similar peak period (8.03 seconds). The resulting wave forces are also 28% the strength of those observed in January. As illustrated in Figures 6 and 7, the predictions are still reasonable but the avearage errors are larger. The largest errors occur at the peaks of the wave force.

While much more investigation could be conducted on the influence of training variables and the seasonal and temporal variation and their impacts on the wave predictions, these results indicate that an LSTM network is able to accurately predict the waves provided sufficient data is available. As such, the predictions are leveraged here to examine the influence of their uncertainty on the control performance.

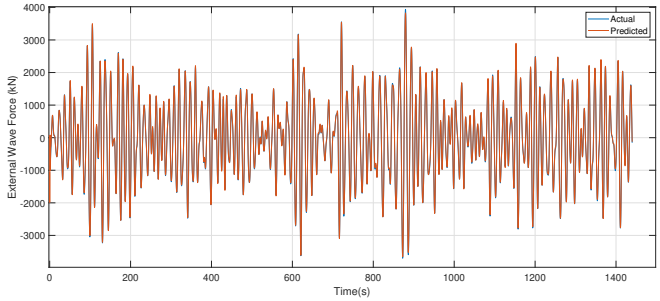

Fig. 4. Actual and predicted wave force for validation data set for Hour 1 of January 1, 2021.

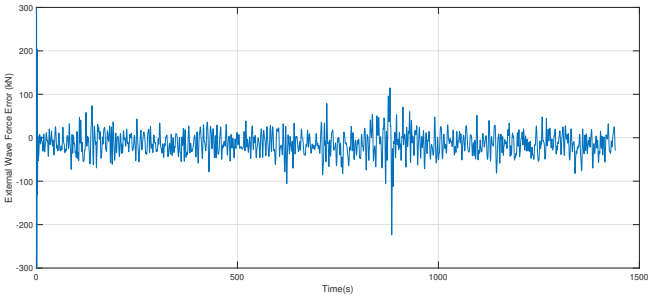

Fig. 5. Prediction error for validation data set for Hour 1 of January 1, 2021.

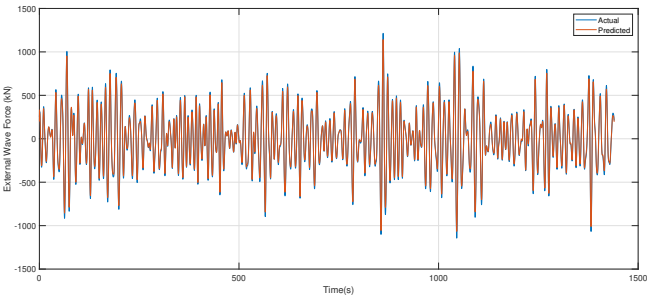

Fig. 6. Actual and predicted wave force for Hour 12 of July 1, 2021 based on the January 1, 2021 trained network.

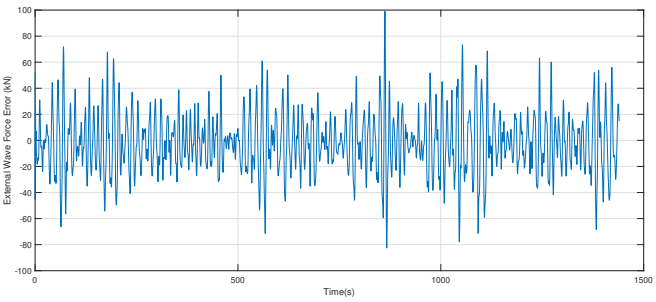

Fig. 7. Prediction Error for Hour 12 of July 1, 2021 Based on the January 1, 2021 Trained Network.

IV. Control Structure and Control Model

The control evaluation was aimed at moving toward a multi-axis system. While most systems operate on a single axis, several multi-axis WECs have been developed such as Pelamis [24] and TALOS [25]. The design here is based on TALOS, which is a point-absorber type WEC with a central heavy mass that is attached to a hull with springs and hydraulic cylinders that form part of the PTO system as illustrated in Figure 8. When the hull is moved by the waves, the relative motion between the central mass and hull drives hydraulic fluid through the PTO system resulting in electricity production. In this work, motions in the vertical or heave direction are considered and the two degree of freedom TALOS system with its moving internal mass and external hull is investigated. Future work will examine the full range of motion of the system.

Fig. 8. TALOS WEC configuration.

Prior work has shown that an MPC structure using position and velocity feedback is effective for this system [26]. A linear MPC structure was effective as long as the controller had knowledge of both the PTO dynamics and hydrodynamics. In prior work, it was assumed that the future wave forces were known for an upcoming time horizon. In this work, the impact of the uncertainty of the wave force predictions is quantified. An MPC was integrated using the model structure shown in Figure 9. The MPC uses a linear model that includes both the hydrodynamics of the WEC and the underlying dynamics of the hydraulic PTO system. A nonlinear MPC could be leveraged but prior work by the authors has shown that nonlinear MPC is computationally expensive for this problem and tends to create drastic actuator commands that could cause excessive wear or damage to the system [26]. The MPC predicts the torque that the PTO should output. This desired torque command is passed on the underlying PTO system. The PTO and hydrodynamics plant models are nonlinear.

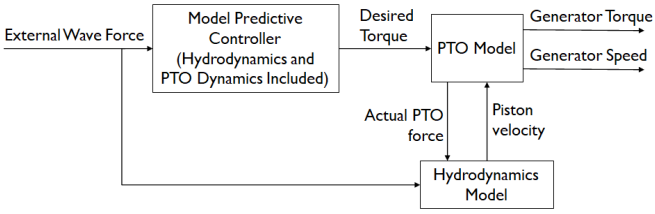

Fig. 9. Full state MPC structure.

To capture the structure of the TALOS device, a two degree of freedom WEC model was created as shown in Figure 10 in which there is a main central mass (ball) and a hull. In the TALOS device, as the mass moves up and down inside the hull, it will pump hydraulic fluid through a circuit driving a generator. The PTO is used to vary the force on the hydraulic piston. For this study, only motion in the vertical or heave direction is considered. The underlying controller aims to maximize the generator power output.

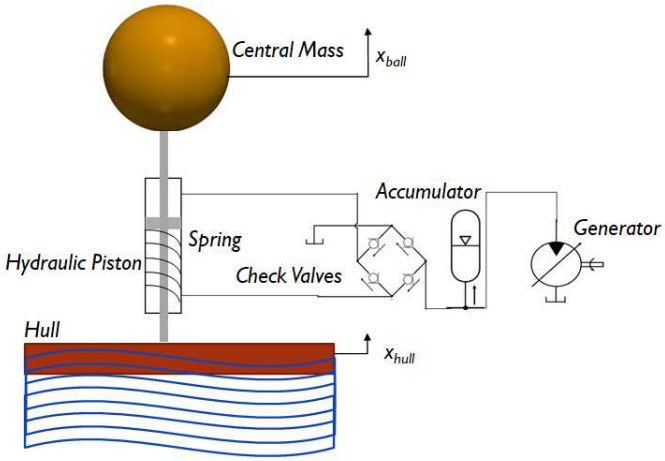

Fig. 10. Two degree of freedom point absorber WEC system with hydraulic PTO

While a summary of the model is provided here, a more thorough discussion is provided in [26]. The hydrodynamics of the point absorber are modeled using standard wave-structure interaction equations including forces due to radiation, buoyancy, drag, and friction as well as the restoring force of the spring, wave excitation force and the force generated by the PTO. Additional forces such as the mooring force may be present but are excluded here.

With the TALOS structure, the hull is impacted by the external wave motion and hydrodynamics while the central ball motion is driven by the hydraulic piston and spring that connect it to the hull. With these forces considered, the motion of the central ball is

$$M_{ball}\ddot{x}_{ball} = -f_{rest} - f_{pto} \tag{1}$$

where M_{ball} is the mass of the ball, x_{ball} is the position of the central mass, f_{rest} is the restoring force from the connecting spring and f_{pto} is the force from the hydraulic PTO system.

The restoring spring force is given by

$$f_{rest} = S_{rest}(x_{ball} - x_{hull}) \tag{2}$$

and is impacted by the relative displacement between the ball and the hull (x_{hull}). The motion of the hull is captured as

$$\begin{aligned}(M_{hull} + m_{\infty,hull})\ddot{x}_{hull} = \quad & -f_{rad} - f_{buoy} - f_{drag} - f_{fric} \\ & +f_{rest} + f_{ext} + f_{pto}\end{aligned} \tag{3}$$

in which M_{hull} is the mass of the hull, $m_{\infty,hull}$ is the added mass, f_{rad} is the radiation force, f_{buoy} is the buoyancy force, f_{drag} is the drag force, and f_{fric} is the friction force. The term f_{ext} represents the external wave force which will leverage the LSTM prediction. The hull leverages the model form used in [27].

The radiation force (f_{rad}) is expressed as a linear state space model with

$$f_{rad} = \mathbf{C}_r\mathbf{q} \tag{4}$$

and

$$\dot{\mathbf{q}} = \mathbf{A}_r\mathbf{q} + \mathbf{B}_r\dot{x}. \tag{5}$$

This model has been shown to accurately capture radiation forces [27], [28].

The buoyancy, drag and friction forces are given by Eqs. 7 and 8, respectively.

$$f_{buoy} = \pi g {R_b}^2 \left(1 - \frac{|x|x}{3{R_b}^2}\right) x \tag{6}$$

$$f_{drag} = 0.5\rho A_w C_d |\dot{x} - v_f|(\dot{x} - v_f) \tag{7}$$

$$\begin{aligned}f_{frict} = \quad & F_n\mu_d tanh(\alpha\dot{x}) + \mu_v\dot{x} \\ & +F_n(\mu_s - \mu_d)e^{-(|\dot{x}|/v_s)^2} tanh(\alpha\dot{x})\end{aligned} \tag{8}$$

In these equations, R_b is the buoy radius, A_w is the submerged surface area of the buoy, C_d is the viscous drag coefficient, and v_f is the water surface velocity in the x direction. The friction model includes F_n representing the normal force, v_s as the Stribeck velocity and μ_d, μ_v, and μ_s representing the damping, viscous and static friction coefficients, respectively.

The system uses a hydraulic PTO system with a model based on the state space model developed by Bacelli et al. [29]. As illustrated in Figure 10, the system has four check valves that rectify the flow as well as a gas accumulator to smooth the flow. The fluid flow drives a hydraulic generator producing power output. The PTO model includes the losses associated with the pressure drops in the pipes, motor leakage and friction. The full model derivation is detailed in [29] and results in two nonlinear differential equations that summarize the PTO dynamics. The first equation captures dynamics of the accumulator volume (V) by

$$\dot{V} = -k_l \cdot P_a(V) - \frac{D}{J} \cdot L + S \cdot (\dot{x_{ball}} - \dot{x_{hull}}) \tag{9}$$

where k_l is a motor leakage coefficient, $P_a(V)$ is the accumulator pressure posed as a function of V, D is the motor constant, J is the inertia momentum of the hydraulic motor shaft, L is the hydraulic motor shaft angular momentum, and S is the piston cross-sectional area.

The dynamics of the generator shaft angular momentum are expressed in the second differential equation for the PTO as

$$\dot{L} = D \cdot \eta_m \cdot P_a(V) - \frac{B}{J} \cdot L - T_G \tag{10}$$

in which η_m is the motor efficiency, B is the motor friction and T_G is the generator torque output.

The PTO force is a function of the accumulator volume and piston velocity as given by

$$\begin{aligned}f_{PTO} \quad & = S \cdot P_a(V) + S \cdot k(S \cdot \dot{x}) \\ & = \tfrac{K_s \cdot (L_g + L_{eq}) \cdot \rho \cdot S \cdot \dot{x}}{2Re \cdot D_h \cdot {A_p}^2} |S \cdot \dot{x}|.\end{aligned} \tag{11}$$

K_S, L_g, L_{eq} and D_h are the pipe cross-section shape factor, geometric pipe length, equivalent length of local resistance and hydraulic diameter of the pipe, respectively. The term ρ represents the density of the hydraulic fluid and A_p is the pipe cross-sectional area.

Combining these equations together, a ten state model was developed with the states [x_{ball} $\dot{x}_{ball}$ q_1 q_2 q_3 q_4 V L x_{hull} $\dot{x}_{hull}$] and the form:

$$\begin{aligned}\dot{x_1} = \quad & x_2 \\ \dot{x_2} = \quad & \tfrac{1}{M_{ball}}(-S_{rs}(x_1 - x_9) - f_{PTO}) \\ \dot{x_3} = \quad & A_{r1} \cdot x_3 + A_{r2} \cdot x_4 + A_{r3} \cdot x_5 + A_{r4} \cdot x_6 + x_{10} \\ \dot{x_4} = \quad & x_3 \\ \dot{x_5} = \quad & x_4 \\ \dot{x_6} = \quad & x_5 \\ \dot{x_7} = \quad & -k_l h(x_7) - \tfrac{D}{J} x_8 + S(x_2 - x_{10}) \\ \dot{x_8} = \quad & D\eta_m h(x_7) - \tfrac{B}{J} x_8 - T_G \\ \dot{x_9} = \quad & x_{10} \\ \dot{x_{10}} = \quad & \tfrac{1}{M_{hull} + m_{\infty,hull}}(-C_{r1} \cdot x_3 - C_{r2} \cdot x_4 - C_{r3} \cdot x_5 \\ & -C_{r4} \cdot x_6 + S_{rest} \cdot (x_1 - x_9) \\ & -\pi g {R_b}^2 \left(1 - \tfrac{|x_9|x_9}{3{R_b}^2}\right) x_9 \\ & -0.5\rho A_w C_d |x_{10} - v_f|(x_{10} - v_f) \\ & -F_n\mu_d tanh(\alpha x_{10}) - \mu_v x_{10} \\ & -F_n(\mu_s - \mu_d)e^{-(|x_{10}|/v_s)^2} tanh(\alpha x_{10}) \\ & +f_{ext} + f_{PTO})\end{aligned} \tag{12}$$

This model was used by the MPC along with the external wave force predictions generated by the LSTM network to examine the control effectiveness. Constraints were integrated to ensure that the ball does not hit the hull and that the torque commands are within a feasible range.

V. Results

Using the control structure depicted in Figure 9, a linear MPC was tested for two scenarios. First, the control effectiveness was examined for January 1st and the performance with the actual wave force data as an input and compared to the scenario when the predicted data was leveraged. Next, the performance was studied for July 1st. In this second case, the controller

effectiveness was compared when leveraging the actual wave force data and when using a prediction based on the LSTM trained on the January 1st data. As seen in Figure 6, the wave force prediction is still quite good but has larger errors at the higher wave forces.

The January cases are able to produce approximately the same power output (with a difference of 0.0015%) when the MPC uses the actual wave force data or the prediction based on the LSTM. Given the relatively small difference between the data and prediction, this minimal difference in performance was expected. Despite similar power production, there are underlying differences in the mass and hull positions, velocities and PTO forces. As seen in Figure 11, the central mass has a similar position when the MPC uses the actual data compared to the prediction. However, when the actual data is used, this leads to the central mass having slightly larger motions. This is likely due to the fact that the LSTM slightly underpredicts the external wave force. In other words, the LSTM tends to predict a lower wave force that the actual leading to a smaller motion of the central mass.

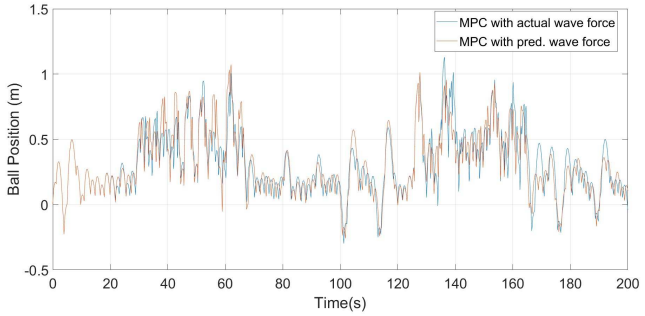

Fig. 11. Position of central mass for January 1, 2021 case with MPC using actual data and predictions.

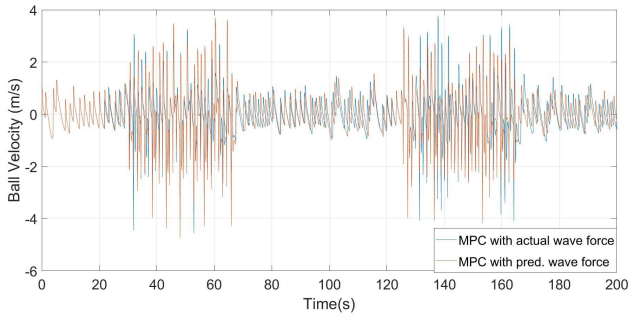

Fig. 12. Velocity of central mass for January 1, 2021 case with MPC using actual data and predictions.

The slightly smaller motions of the central mass also lead to lower velocities although the differences are minor as illustrated in Figure 12. This figure also illustrates the fact that the MPC is tending to optimize the power output by periodically limiting the motion of the mass. Velocities alternate between staying between -1 to 1 m/s and going into a mode with more extreme motion from -4 to 4 m/s. This behavior appears to be in part due to the controller having difficulty solving within the system constraints.

The constraints require a positive distance between the central mass and hull, but since it is preferable to keep some additional buffer, a constraint of 0.05m was imposed. As observed in Figure 13, in both MPC cases, the controller struggles to find a solution that abides by this constraint. During times when it is unable to keep the distance consistently above 0.05m, the control action calls for smaller PTO forces (Figure 14) that keep the central mass velocity low. When the MPC is able to largely maintain the constraint, it has larger control action resulting in larger velocities and power outputs. The wave prediction error does not seem to exaggerate this issue as both MPC options have a similar challenge.

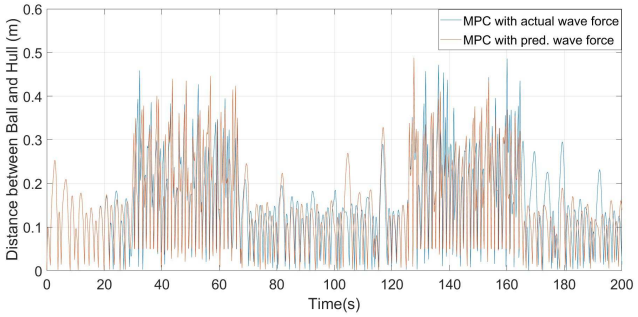

Fig. 13. Distance between central mass and hull for January 1, 2021 case with MPC using actual data and predictions.

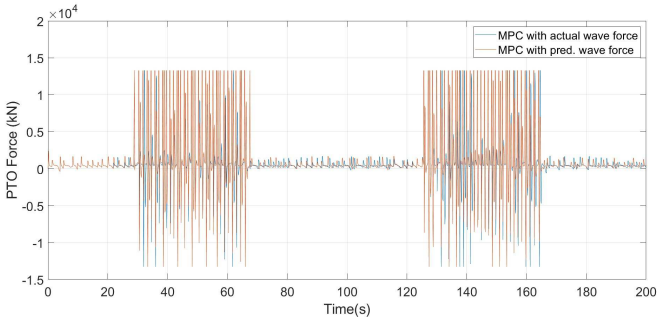

Fig. 14. PTO force for January 1, 2021 case with MPC using actual data and predictions.

The July cases also have minimal changes in power output although the difference is more significant than in the January cases where the MPC is trained on the data from that time frame. For the July 1st case, a similar power output is achieved (with a difference of 0.064%) when the MPC uses the actual wave force data or the prediction based on the LSTM. In the July cases, the wave prediction has more error, but since it tends to under-predict the motion this tends to lead to slightly more conservative control action. The central mass motion is slightly more limited when the predicted wave forces are used by the MPC as seen in Figure 15. As illustrated in Figures 16 and 17, the velocities and distances maintained between the central mass and hull are also slightly lower when the MPC uses the predicted wave forces rather than the actual values. As in the January cases, the July cases also exhibit a fluctuating behavior with the controller being conservative at times due to challenges with the constraints. During

these points where constraint violation is high, the PTO force again exhibits low values (Figure 18. PTO action is higher and power output is higher at points when larger distances between the central mass and hull are able to be maintained.

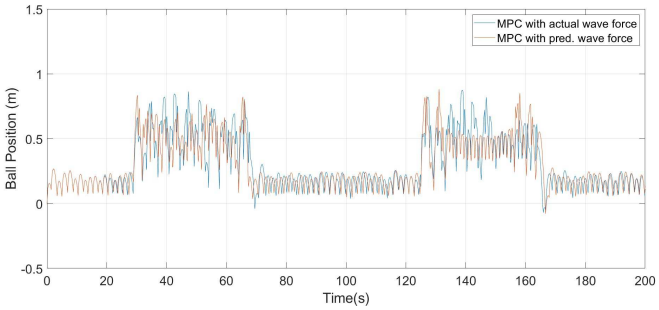

Fig. 15. Position of central mass for July 1, 2021 case with MPC using actual data and predictions.

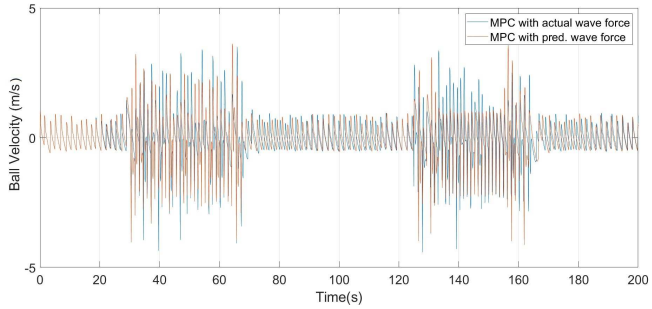

Fig. 16. Velocity of central mass for July 1, 2021 case with MPC using actual data and predictions.

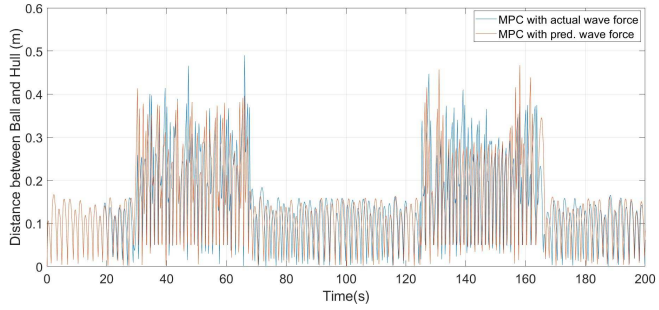

Fig. 17. Distance between central mass and hull for July 1, 2021 case with MPC using actual data and predictions.

Despite significant differences in wave force between January and July, both cases produce similar power output. This is because the wave forces in January are large enough that the WEC appears to not be able to fully take advantage of them due to the underlying constraints between the central mass and the hull. In both cases slight differences in power output are observed when the predictions are used instead of the actual data, but these differences are quite minimal. As illustrated in Figure 19, the energy output is quite similar when the MPC uses either the actual or predicted wave force data and despite the larger incoming wave forces in January, one hour in both January and July produce similar energy outputs. As

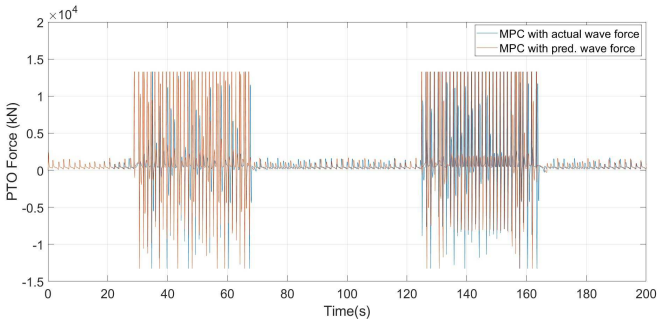

Fig. 18. PTO force for July 1, 2021 case with MPC using actual data and predictions.

such, constraints appear to be a bigger limiting factor on the WEC power output and the uncertainty of the incoming wave produces only a minor effect.

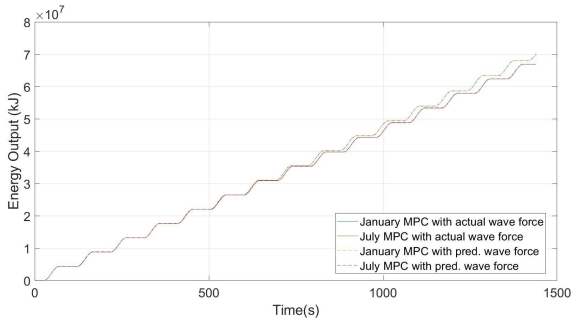

Fig. 19. Energy output using actual data and predictions.

These results indicate that an LSTM trained on a relatively small amount of data may be able to provide accurate predictions for future cases. However, the current analysis is limited since high resolution data had to be recreated due to the unavailability of raw data at a high resolution. In this work, hourly experimental statistical metrics were used to recreate the 10Hz data using an assumed random behavior within a wave spectrum to create the irregular wave characteristics.The data used for the prediction is created via the same algorithm in both cases and as such reduces the variability from that likely observed in the real case. As observed in Figures 2 and 3, the hourly statistics of wave characteristics can change dramatically over the course of a day and from season to season. Future work should examine the impact of seasonal and temporal variation using experimentally obtained data. In addition, factors including LSTM hyperparameter tuning and the MPC prediction horizon will influence the results and their influence should be explored.

VI. Conclusions

This study illustrated that an LSTM network can capture external wave forces and slight inaccuracies in the predictions do not significantly degrade performance for the two degree of freedom WEC system examined in this work. With a more complex WEC design like that of TALOS, constraints are a challenge and this study illustrates that those constraints can significantly limit the controller's ability to optimize performance.

Future work will focus on including additional degrees of freedom to the motion and incorporating higher resolution experimental data as it becomes available.

REFERENCES

[1] J. V. Ringwood, G. Bacelli, and F. Fusco, "Energy-maximizing control of wave-energy converters: The development of control system technology to optimize their operation," *IEEE control systems magazine*, vol. 34, no. 5, pp. 30–55, 2014.

[2] A. Têtu, *Power Take-Off Systems for WECs*. Cham: Springer International Publishing, 2017, pp. 203–220. [Online]. Available: https://doi.org/10.1007/978-3-319-39889-1_8

[3] J. Hals, J. Falnes, and T. Moan, "A Comparison of Selected Strategies for Adaptive Control of Wave Energy Converters," *Journal of Offshore Mechanics and Arctic Engineering*, vol. 133, no. 3, 03 2011, 031101. [Online]. Available: https://doi.org/10.1115/1.4002735

[4] D. García-Violini, N. Faedo, F. Jaramillo-Lopez, and J. V. Ringwood, "Simple controllers for wave energy devices compared," *Journal of Marine Science and Engineering*, vol. 8, no. 10, p. 793, 2020.

[5] J. A. Cretel, G. Lightbody, G. P. Thomas, and A. W. Lewis, "Maximisation of energy capture by a wave-energy point absorber using model predictive control," *IFAC Proceedings Volumes*, vol. 44, no. 1, pp. 3714–3721, 2011.

[6] G. Li and M. R. Belmont, "Model predictive control of sea wave energy converters–part i: A convex approach for the case of a single device," *Renewable Energy*, vol. 69, pp. 453–463, 2014.

[7] R. Genest and J. V. Ringwood, "Receding horizon pseudospectral control for energy maximization with application to wave energy devices," *IEEE Transactions on Control Systems Technology*, vol. 25, no. 1, pp. 29–38, 2016.

[8] D. Garcia-Violini and J. V. Ringwood, "Energy maximising robust control for spectral and pseudospectral methods with application to wave energy systems," *International Journal of Control*, vol. 94, no. 4, pp. 1102–1113, 2021.

[9] G. Li, "Nonlinear model predictive control of a wave energy converter based on differential flatness parameterisation," *International Journal of Control*, vol. 90, no. 1, pp. 68–77, 2017.

[10] N. Faedo, G. Scarciotti, A. Astolfi, and J. V. Ringwood, "Energy-maximising control of wave energy converters using a moment-domain representation," *Control Engineering Practice*, vol. 81, pp. 85–96, 2018. [Online]. Available: https://www.sciencedirect.com/science/article/pii/S0967066118304246

[11] ——, "Nonlinear energy-maximizing optimal control of wave energy systems: A moment-based approach," *IEEE Transactions on Control Systems Technology*, vol. 29, no. 6, pp. 2533–2547, 2021.

[12] U. Korde, "Efficient primary energy conversion in irregular waves," *Ocean engineering*, vol. 26, no. 7, pp. 625–651, 1999.

[13] F. Fusco and J. V. Ringwood, "Short-term wave forecasting for real-time control of wave energy converters," *IEEE Transactions on sustainable energy*, vol. 1, no. 2, pp. 99–106, 2010.

[14] S. Shi, R. J. Patton, and Y. Liu, "Short-term wave forecasting using gaussian process for optimal control of wave energy converters," *IFAC-PapersOnLine*, vol. 51, no. 29, pp. 44–49, 2018.

[15] F. Fusco and J. V. Ringwood, "Short-term wave forecasting with ar models in real-time optimal control of wave energy converters," in *2010 IEEE International Symposium on Industrial Electronics*. IEEE, 2010, pp. 2475–2480.

[16] Y. Lao and J. T. Scruggs, "Robust control of wave energy converters using unstructured uncertainty," in *2020 American Control Conference (ACC)*. IEEE, 2020, pp. 4237–4244.

[17] S. Lattanzio and J. Scruggs, "Maximum power generation of a wave energy converter in a stochastic environment," in *2011 IEEE international conference on control applications (CCA)*. IEEE, 2011, pp. 1125–1130.

[18] M. T. Sichani, J.-B. Chen, M. Kramer, and S. R. Nielsen, "Constrained optimal stochastic control of non-linear wave energy point absorbers," *Applied Ocean Research*, vol. 47, pp. 255–269, 2014.

[19] T. Sun and S. R. Nielsen, "Stochastic control of wave energy converters for optimal power absorption with constrained control force," *Applied Ocean Research*, vol. 87, pp. 130–141, 2019.

[20] T. Sun, S. R. Nielsen, and B. Basu, "Stochastic control of wave energy converters with constrained displacements for optimal power absorption," *Applied Ocean Research*, vol. 89, pp. 1–11, 2019.

[21] S. C. James, Y. Zhang, and F. O'Donncha, "A machine learning framework to forecast wave conditions," *Coastal Engineering*, vol. 137, pp. 1–10, 2018.

[22] L. Li, Z. Yuan, and Y. Gao, "Maximization of energy absorption for a wave energy converter using the deep machine learning," *Energy*, vol. 165, pp. 340–349, 2018. [Online]. Available: https://www.sciencedirect.com/science/article/pii/S0360544218318577

[23] L. Li, Y. Gao, D. Ning, and Z. Yuan, "Development of a constraint non-causal wave energy control algorithm based on artificial intelligence," *Renewable and Sustainable Energy Reviews*, vol. 138, p. 110519, 2021. [Online]. Available: https://www.sciencedirect.com/science/article/pii/S1364032120308042

[24] R. P. M. Parker, G. Harrison, and J. Chick, "Energy and carbon audit of an offshore wave energy converter," *Proceedings of the Institution of Mechanical Engineers, Part A: Journal of Power and Energy*, vol. 221, no. 8, pp. 1119–1130, 2007.

[25] G. Aggidis and C. Taylor, "Overview of wave energy converter devices and the development of a new multi-axis laboratory prototype," *IFAC-PapersOnLine*, vol. 50, no. 1, pp. 15 651–15 656, 2017.

[26] C. M. Hall, Y. Wu, W. Sheng, and G. Aggidis, "The impact of control structure and constraints on the performance of a wave energy converter with a hydraulic pto system," in *Proceedings of the 2023 International Society of Offshore and Polar Engineers Conference*, 2023.

[27] M. Jama, B. F. Mon, A. Wahyudie, and S. Mekhilef, "Maximum energy capturing approach for heaving wave energy converters using an estimator-based finite control set model predictive control," *IEEE Access*, vol. 9, pp. 67 648–67 659, 2021.

[28] T. Duarte, A. Sarmento, M. Alves, and J. Jonkman, "State-space realization of the wave-radiation force within fast," National Renewable Energy Lab.(NREL), Golden, CO (United States), Tech. Rep., 2013.

[29] G. Bacelli, J.-c. Gilloteaux, and J. Ringwood, "State space model of a hydraulic power take off unit for wave energy conversion employing bondgraphs," *Proc. World Renewable Energy Conference, Glasgow*, 01 2008.